1-pT noise fluxgate magnetometer for geomagnetic measurements and unshielded magnetocardiography

Michal Janosek
Dept. of Measurement
Czech Technical University in Prague
Prague, Czech Republic
janosem@fel.cvut.cz

Mattia Butta
Dept. of Measurement
Czech Technical University in Prague
Prague, Czech Republic
buttamat@fel.cvut.cz

Michal Dressler
Dept. of Measurement
Czech Technical University in Prague
Prague, Czech Republic
dressmic@fel.cvut.cz

Elda Saunderson
Directorate Space Science
South African National Space Agency
Hermanus, South Africa
esaunderson@sansa.org.za

David Novotny
Dept. of Measurement
Czech Technical University in Prague
Prague, Czech Republic
novotd12@fel.cvut.cz

Coenrad Fourie
Dept Electrical and Electronic Engineering
Stellenbosch University
Stellenbosch, South Africa
coenrad@sun.ac.za

***Abstract*— We present the development of a low-noise, fundamental-mode, orthogonal fluxgate magnetometer with four amorphous, annealed ferromagnetic wires. The 1-Hz noise obtained in open-loop and closed-loop is as low as 0.75 and 1.5 $pT_{rms}/\sqrt{Hz}$, respectively, with white noise level about 0.6 $pT_{rms}/\sqrt{Hz}$. This is to our knowledge the lowest figure published for a fluxgate magnetometer so far. By using the annealed sensor cores, we also found the offset drift to decrease approx. 6-times to 2.5 nT/K. We compared the instrument performance to a low-noise observatory magnetometer when doing geomagnetic measurements and show that it is fully suitable for measurements at mHz frequencies, e.g. magnetotellurics. The magnetometer performance enables room-temperature, unshielded magnetocardiography. With a gradiometric arrangement of two sensors, we were able to perform a MCG measurement in ambient field and even without averaging, the signal could be clearly resolved.**

Keywords*— *fluxgate, noise, fundamental-mode

I. Introduction

Low-noise fluxgate magnetometers (with amplitude noise density below 10 $pT_{rms}/\sqrt{Hz}$) are mostly built as instruments for measuring weak magnetic fields in the Earth's field range (up to 50 µT). They are used at geomagnetic observatories [1], for navigation and prospection [2], attitude correction and scientific experiments in aerospace [3], in magnetotellurics [4][5], non-destructive testing and evaluation [6], nanoparticle detection [7] and in other subjects, where vectorial response to magnetic fields and a room-temperature operation are required. Low-noise sensors were used even for shielded magnetocardiography [8][9]. Fig. 1 shows the requirements for these applications - it is evident that 1-pT performance would be beneficial, together with the desired frequency range of about 1 mHz to 100 Hz.

As for parallel-type fluxgates, the state-of-the art magnetometers exhibit noise level about 3-4 $pT_{rms}/\sqrt{Hz}$ at 1 Hz [9][11][12]. 1-pT noise was obtained with cross-correlation measurements and special sensor arrangement in [13], however the principle was not exploited any further. Design requirements to use such a low-noise sensor in an observatory variometer were discussed recently in [14].

The other branch of fluxgate sensors, the orthogonal-type, brings low-noise performance only with the fundamental-mode operated fluxgates. They were introduced by Sasada in 2001 [15] and since then the parameters have continuously improved – the noise decreased from the initial 10 pT down to about 1.5-2 $pT_{rms}/\sqrt{Hz}$ for laboratory devices [17]; with the help of core annealing, sub-pT noise was reported recently [18].

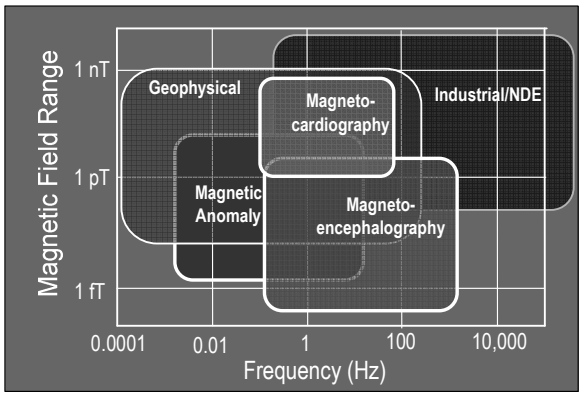

Fig. 1. Overview of applications of 1-pT level sensors - from [16]

We have to state that the generally accepted disadvantage of fundamental-mode fluxgates is their offset-drift - about 50 nT/K was shown in [17]. This was addressed previously and solutions were implemented either in digital or analog domain [19]-[21] – 0.7 nT stability within a 60 °C range was shown in [20]. However, we decided not to use any of these techniques, because they tend to increase noise.

In this article, we show the peculiarities of embedding such a low noise fluxgate sensor in a practical magnetometer for real-world measurements out of the laboratory. The achieved noise is actually so low, that we were able to perform a magnetocardiography experiment in ambient field.

This article is an extended version of the proceedings article [22] with additional details and results.

II. SENSOR MANUFACTURING

For the fluxgate sensor core, we used Unitika 125AC20 amorphous wires of 125 µm diameter, with chemical composition $(Co_{0.94}Fe_{0.06})_{72.5}Si_{12.5}B_{15}$.

The sensor was manufactured in two versions: as-cast and joule-annealed [18] - annealing and increasing the effective cross-section improved the sensitivity and decreased the magnetic noise (our initial results in [22] used only as-cast, two-wire sensor). The amorphous wires form a "Π-shaped" circuit on a FR-4 printed circuit board - see Fig. 2. In order to further decrease the noise, the FR-4 board with the sensor core was embedded in silicone providing thermal damping [23]. The pick-up (also compensation) coil was wound with multiple layers on a ceramic tube, with approx. 1600 and 2000 turns for the as-cast and annealed core, respectively. The core of the annealed sensor was approx. 1 cm longer than of the as-cast one - see Fig. 3. When tuned to the working frequency (cca 47 kHz), and with excitation current of 100 mA p-p and 48 mA AC and DC value, respectively, the sensor sensitivity was about 170 kV/T.

As the fundamental-mode fluxgate operates at a relatively high excitation frequency, the sensor wiring is critical and sensitive to capacitive pickup e.g. from lights with electronic ballasts etc. We used subminiature, PTFE insulated cable with two twisted-shielded pairs - for excitation and pickup. Balancing and/or shielding the common-mode were found to be critical in the instrument design, as it will be shown later.

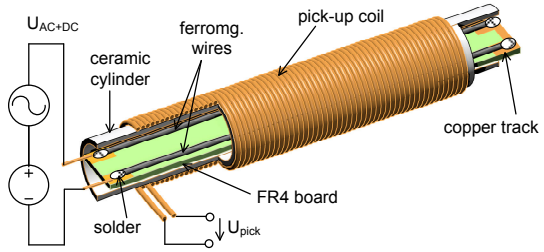

Fig. 2. Sensor structure – 2 ferromagnetic wires are soldered to a FR-4 printed-circuit-board, forming a "Π shape", and inserted in a ceramic cylinder (silicone filling not shown) with the pick-up coil. The excitation voltage U_{AC+DC} is connected to the ferromagnetic wires.

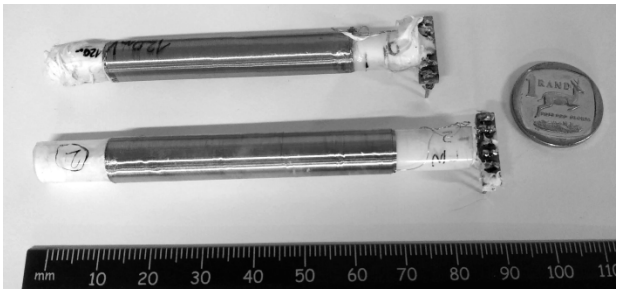

Fig. 3. Photo of manufactured sensors - both the two-wire, as-cast sensor (top) and the 4-wire, annealed one (bottom) are shown.

III. ELECTRONICS DESIGN

A practical magnetometer should meet the noise figures obtained in the laboratory. For the annealed sensors, the laboratory results indicated about 0.7 $pT_{rms}/\sqrt{Hz}$ at 1 Hz [18].

The electronics relies on a precise direct-digital-synthesis (DDS) waveform-generator chip AD 9106 and a precise, feedback-loop stabilized power stage. The electronics block diagram is shown in Fig. 4 and its individual parts are thoroughly described in [22].

In the following paragraphs, we will concentrate on a few critical points and changes in the design which had to be addressed during the transition to annealed, sub-pT sensors.

A. *Parasitic coupling of the excitation signal*

Because we did not use any push-pull technique for the excitation generator, our excitation is inherently single ended, thus asymmetric with respect to ground. A large AC common voltage (about 3.2 V_{p-p} for annealed wires) is present along the excitation wires, with possible coupling to the wiring of the input coil. This is a disadvantage of first harmonic fluxgates when compared to second harmonic types, where the excitation and useful signal are not at the same frequencies simplifying the wiring and balancing. This excitation-to-pickup coupling will in turn result in offsets, and their instability will manifest as low-frequency noise. To keep the offsets in nT-range, we had to use common-mode chokes for decoupling the inputs and the excitation, and we had to use a fast differential amplifier built with LT6234 for amplifying the input signal.

B. *Capacitive coupling of ambient common-mode noise*

The sensitivity of our annealed sensors is about 200 kV/T at 47 kHz and 100 kHz for the annealed and as-cast sensors, respectively, which for 1 pT results in 200 nV useful signal. We have found that even when running on batteries, carefully balancing our differential amplifier with precise resistors and using common mode chokes and twisted shielded leads, it was finally necessary to shield the sensor with an aluminium foil to obtain 1 $pT_{rms}/\sqrt{Hz}$ and better performance. By wrapping the sensor in a thin conductive foil, we were able to suppress most of the capacitive (common-mode) coupling of unwanted signal to the differential amplifier via the sensor wiring - Fig. 5 demonstrates the solution.

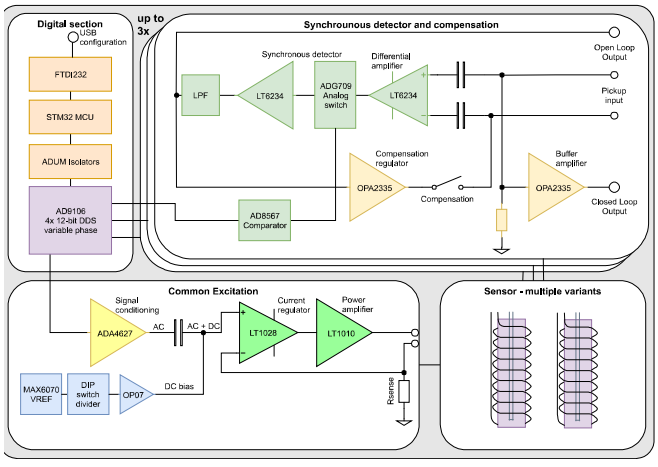

Fig. 4. Block diagram of the magnetometer electronics. A single channel is shown, the excitation stage is common for all sensors in series.

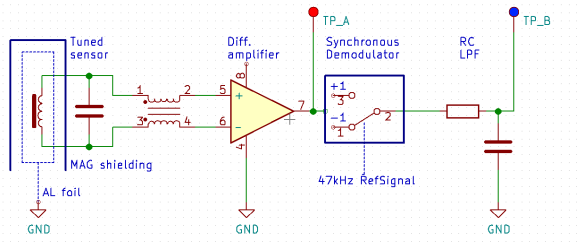

Fig. 5. Detail of the front-end circuitry with sensor wrapped by a grounded aluminium foil.

We verified this problem by observing the differential amplifier output – TP_A test point in Fig. 5 - with the excitation switched off, i.e. the sensor acted as an antenna only and we were observing only the effect of EMI coupling. Theoretically, with perfect differential amplifier and infinite common-mode rejection, we would not observe any signal when in the magnetic shield. However, as seen in Fig. 6, connecting the Al foil shield to instrument ground was necessary to reduce the amplified EMI even in the shielding.

In Fig. 7, we see the noise spectra when such a parasitic signal is demodulated by the synchronous detector of our magnetometer - again we see that connecting the Al foil shield to the instrument ground is beneficial. Moreover, we could verify that the majority of unwanted noise is due to capacitive coupling - with the sensor in the magnetic shield, the actual noise signal increased because of the metallic0 shield plates. Any induced EMI by magnetic coupling would be eliminated in the shield. Thus, for any further operation, we decided to use the aluminium shielding foil, since it does not introduce any significant bandwidth restriction and provides efficient shielding from capacitively coupled EMI. Also, an alternative excitation frequency should be chosen in areas with high EMI. Because of the switching synchronous detector which behaves as a comb filter on odd-harmonics of the switching frequency, not only the first but also the 3rd harmonic should stay out of local EMI (see Fig. 6).

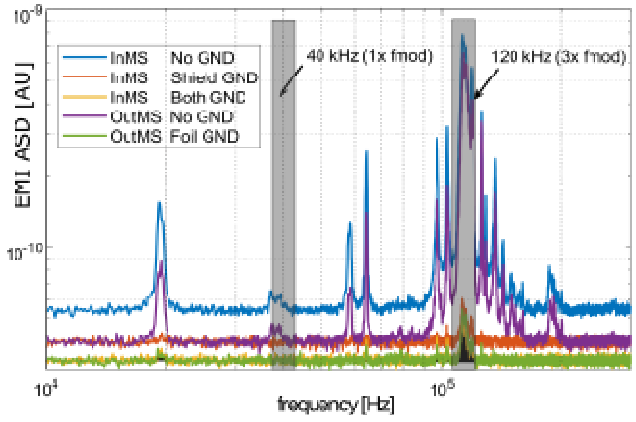

Fig. 6. Spectrum of EMI at the pick-up coil (after amplification) - excitation is off, sensor is an EMI antenna only. (TP A of Fig. 5)

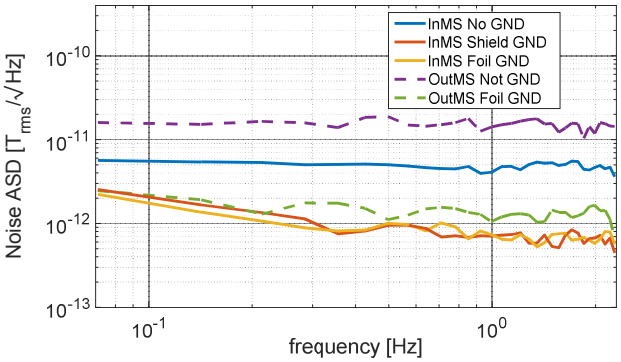

Fig. 7. Demodulated EMI in magnetic units (excitation off) in and out of the magnetic shield (In/OutMS) – TP-B of Fig. 5. Various grounding configurations shown – no ground or mag. shield or Al foil were grounded. The 0.7 pT limits the magnetometer performance.

C. *Closed loop operation*

Originally, for closing the feedback loop, we used OPA2335 amplifier as an integrator [22]. The choice of this particular amplifier was unfortunate because of its high voltage noise, despite its excellent DC properties and low bias current. This broadband noise was actually coupled through the pickup/compensation coil itself: the coil constant is about 26 nT/μA. With a 1 kΩ resistor in the feedback loop and anticipated amplification of the error signal G = 1, the 60 nV white amplifier noise results in:

$$(60\ \text{nV}/1000\Omega) \times (26\ \text{nT}/\mu\text{A}) \cong 1.6\ \text{pT} \qquad (1)$$

By replacing the op-amp with another type (LTC2058) with 5× lower noise, we would be able to obtain a theoretical noise floor of 0.32 pT. However, as shown later for annealed sensors, this noise limit in a feedback loop was not met and it is understood to occur due to imbalance of the pick-up coil with respect to ground, which happens when closing the single-ended feedback loop, thus decreasing the achievable CMRR.

D. *Output signal digitizer*

The output of the magnetometer is analog with ± 2.5 V range corresponding to ± 12 μT in open-loop (with annealed sensor), or ± 25 μT in closed loop (with as-cast sensor).

For the geomagnetic measurements, we used a 24-26 bit DAQ module type “AD-USB24” manufactured by Janascard [24] for data conversion and acquisition. This module uses a custom dual-slope integrating analog-to-digital converter and is galvanically isolated from the USB bus. Moreover, it employs a unique input “chopping” function to avoid the influence of parasitic thermoelectric voltages and uncorrelated noise [25]. The integrating time t_{int} and USB latency limits the bandwidth of the digitized signal, for 80-ms integration time and 2-samples chopping, our bandwidth was about 2 Hz (220 ms sampling time). When using gain of 102× (approx. 100 nT range), the equivalent 1-Hz noise was about 50 fT/√Hz, whereas for gain of 2× (full magnetometer range of ± 2.5V), the noise was 0.7 $pT_{rms}/\sqrt{Hz}$ - see Fig. 8. It can be also seen that without chopping, the low-frequency noise increases even with t_{int}=320ms.

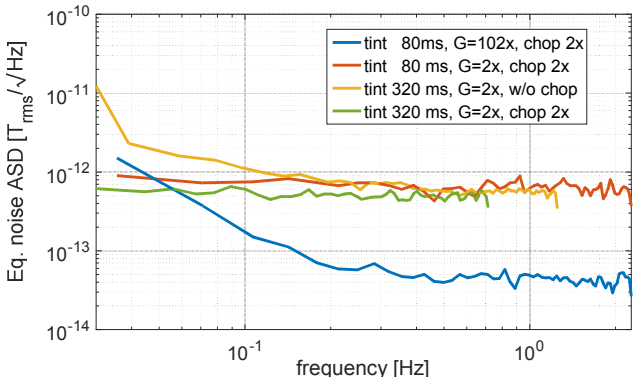

Fig. 8. Equivalent noise of AD-USB24, shown for different gains (2× and 102×), 80ms and 320ms integration with and without chopping.

For MCG measurements, where the required bandwidth is higher (about 20 Hz), the outputs of the two channels of the magnetometer were digitized using a NI PXIe-4303 data acquisition card connected to a regular desktop PC. This digitizer features simultaneous 24-bit analog-to-digital converters and a maximum sampling frequency of 51.2 kHz.

E. The finished instrument and its noise performance

The magnetometer in its improved second version as compared to [22] is powered by either an external power-supply or 12V rechargeable battery. Fig. 9 depicts the magnetometer box open to show the electronic board.

The 1-Hz noise of the magnetometer with as-cast sensors was measured in a 6-layer shield and was about 1.5 $pT_{rms}/\sqrt{Hz}$ [22]. Noise with the annealed sensors was then measured in a three-layer Permalloy shielding chamber at SANSA Space Science; the shielding factor of about 1000 was enough thanks to the low ambient field noise, which is below 100 $pT_{rms}/\sqrt{Hz}$ even in a laboratory.

Fig. 10 shows the noise performance with an annealed sensor, as measured with the Janascard DAQ and a gain of 512×. In open-loop, the noise was 0.8 $pT_{rms}/\sqrt{Hz}$ at 1 Hz with approx. 0.6 pT noise floor. In closed loop, the 1-Hz noise deteriorated to 1.5 $pT_{rms}/\sqrt{Hz}$, however at 100 mHz it is 2.5 $pT_{rms}/\sqrt{Hz}$, which is the same as in open-loop. The DAQ noise was negligible on this range (tens of $fT_{rms}/\sqrt{Hz}$).

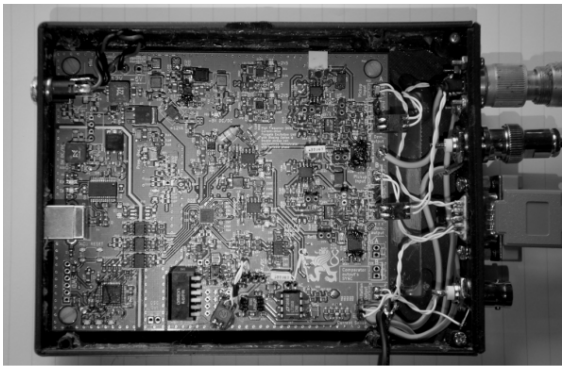

Fig. 9. Magnetometer box shown open. Single printed-circuit board with the electronics provides all functions as of Fig.4.

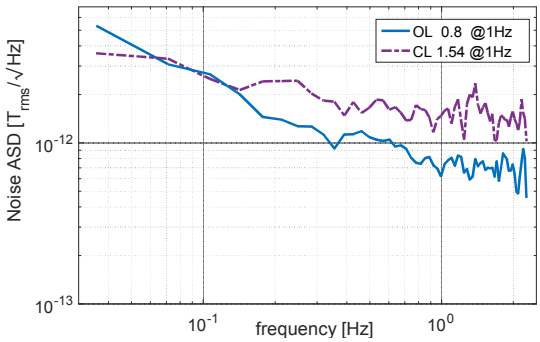

Fig. 10. Noise performance with annealed sensor in open and closed loop.

F. Offset drifts with temperature

Temperature drift of magnetometer offset was established in a non-magnetic, unshielded chamber, where the sensor head was placed in the E-W direction and temperature swept between room temperature and 33 °C. Because the observed drift was much larger than the change in Earth's field during the measurement, unshielded measurement was sufficient.

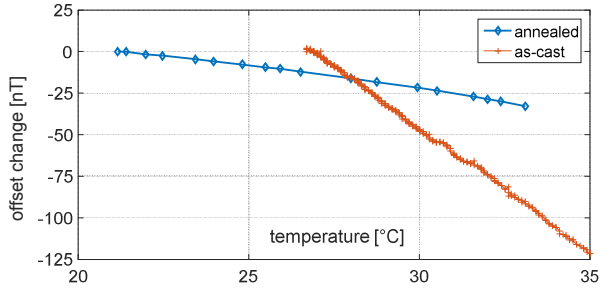

Fig. 11. Offset drift measured in a non-magnetic thermostated box (sensor head was heated) for the annealed and as-cast sensor.

The offset temperature coefficient was established as a local derivative of the offset temperature dependencies – see Fig. 11. For the annealed sensor it was as approx. −2.5 nT/K, which is better than −15 nT/K with an as-cast sensor, and better than 50 nT/K reported previously [20].

IV. Geomagnetic Measurements at SANSA Space Science

A. The instruments at SANSA - SQUID and 1-s observatory magnetometer LEMI-025

SANSA Space Science, located in Hermanus, South Africa (INTERMAGNET designation HER) operates an unshielded, HTS (LN_2) DC SQUID system, in collaboration with Stellenbosch University and LSBB in Rustrel, Provence, France [26]. Currently, two axes (horizontal and vertical) are running and the SQUID is measuring geomagnetic field variations [27].

However, as shown previously in our proceedings article [22], the SQUID noise was found to be much higher than anticipated. Even though zero-field cooling and EMI-enhancement techniques were utilized, we were not able to reach the manufacturer noise of 0.3 $pT_{rms}/\sqrt{Hz}$ at 1 Hz; it was actually about 6 and 20 $pT_{rms}/\sqrt{Hz}$ in X-axis and Z-axis, respectively (Z-axis is more noisy due to local disturbances).

For the purpose of a low-noise geomagnetic comparison, we are thus comparing our measurements only to the LEMI-

025 observatory magnetometer, manufactured by the Institute for Space Research in Lviv, Ukraine, with a sampling frequency of 1 Hz and resolution of 10 pT. The claimed noise level is <10 $pT_{rms}/\sqrt{Hz}$ and 3 $pT_{rms}/\sqrt{Hz}$ at 0.1 and 1 Hz, respectively, which is the state-of-the-art in this field [14][28].

B. *Comparison methodology*

The general difficulty when comparing two vectorial measurements is their alignment. However, for a longer record of geomagnetic field, diurnal variations and magnetic field fluctuations can be used to mutually align the instruments. The disadvantage of numerical alignment is however propagation of noise from any noisy axis to the other axes. In the case of geomagnetic measurements with anthropogenous noise, the noisiest axis is the vertical one. Thus, numerical "tilting" of the coordinates and noise computation should be avoided, e.g. by precisely leveling the sensor. Numerical rotation in the horizontal plane will not deteriorate the results in terms of noise, since the local noise in E-W and N-S axes is approximately the same.

For this comparison, we used a single sensor mounted on the Askania circle in the "quiet" hut located approx. 50 m away from the next building and 100 m away from the main building area. The magnetometer was powered by batteries and the USB DAQ unit was connected to a battery-operated laptop PC, approx. 5-m away, see Fig. 12.

The horizontal sensor was rotated to the E-W direction, where the noise at SANSA is lowest. Also, we can then set the gain of our DAQ to 102× (range about ± 70 nT) to obtain the noise floor as low as possible. We thus rotated it to coincide with the magnetic E-W direction (~0 nT), since the component in the geographic E-W direction is about −4700 nT in Hermanus. The approximate vertical alignment was done with the help of spirit levels.

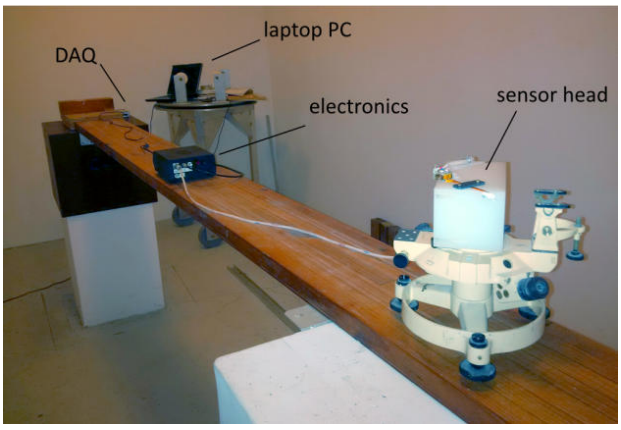

Fig. 12. Sensor placement in the "quiet" hut. The laptop-PC with the USB DAQ logger are at a distance of 5 m.

In order to numerically align the axis of the of 1-pT magnetometer to LEMI-025, the following optimization problem has been solved:

$$B_R = [\sin(\theta)\cos(\varphi) \quad \sin(\theta)\sin(\varphi) \quad \cos(\theta)] \begin{vmatrix} B_{25x} \\ B_{25y} \\ B_{25z} \end{vmatrix} \qquad (1)$$

$$B_R - B_{1px} - O_{1px}(1 + \tau_x * t) = \min \qquad (2)$$

$\mathbf{B}_{25}$ is the magnetic flux density (*x*, *y* and *z* components) as measured with LEMI-025, B_R is the rotated horizontal (EW) field vector component. B_{1px} is the x-axis component as measured with the 1-pT instrument, O_{1px} is its initial offset and τ_x is the offset temperature coefficient in this axis. In addition to our initial results in [22], we also added the tilting angle θ, because the sensor was not perfectly horizontal. However, for the reasons described above, for noise calculations, we assumed the tilting angle to be θ=0 not to introduce any noise from the noisy vertical component into the comparison.

As we see in Eq. 2, because we were not able to measure the temperature of the sensor head without disturbing the magnetic field, we decided to estimate that the offset drift within a 3-hour recording window is linear, and we fitted on the sample time rather than temperature. The fitted coefficient τ was about 0.2 pT/s.

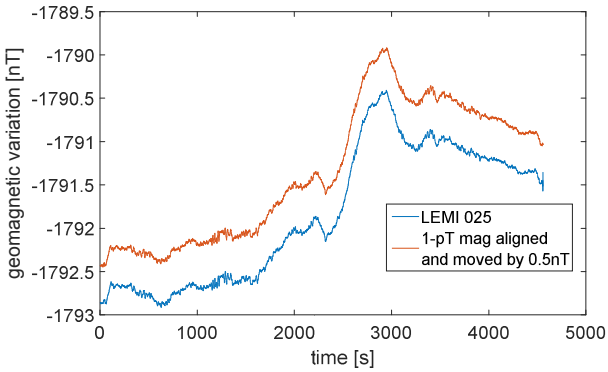

Fig. 13. Alignment of LEMI-025 and 1-pT fluxgate E-W axis sensor. LEMI data offset by 0.5 nT for clarity (17/09/2018).

The optimization problem was solved in MATLAB with *fminsearch* function and the resulting alignment is shown in Fig. 13. From that result we can conclude that even when the sensor drifts in its offset inherently, we can compensate for it and use it even for ultra-low frequency (mHz) measurements.

C. *Geomagnetic measurement - as-cast sensor*

The results of geomagnetic measurements with the as-cast sensor are shown in Fig. 14 (night-time data was used because of the anthropogenous noise during the day). The 1-pT sensor was placed in the "quiet hut" as in Fig. 12. From the comparison with simultaneously obtained observatory magnetometer data, we see that the LEMI-025 noise is limited by about 6 $pT_{rms}/\sqrt{Hz}$ for frequencies above 0.3 Hz. This can be either due to the instrument noise itself, or by higher field noise at the LEMI-025 position - its "instrument bunker" is about 100-m from other buildings which might generate local noise. For lower frequencies, measurement with both instruments results in the same noise (about 15 $pT_{rms}/\sqrt{Hz}$ @ 100 mHz).

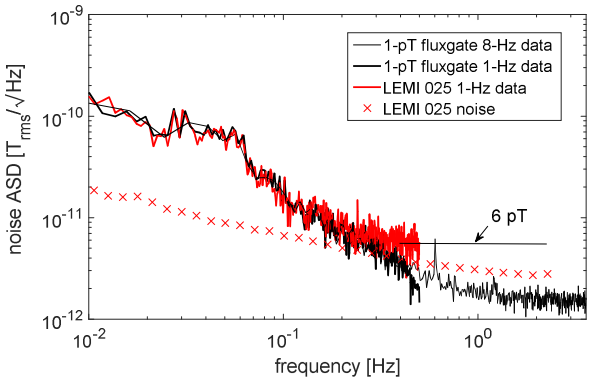

Fig. 14. Geomagnetic field noise spectra as measured with the as-cast sensor and LEMI-025 (17/09/2018). At 1 Hz, 2 $pT_{rms}/\sqrt{Hz}$ was obtained. LEMI-025 noise limit [14] is shown with crosses.

D. 1-pT geomagnetic measurement - annealed sensor

We repeated the geomagnetic measurements once more with an annealed sensor to verify the possibility of (sub) pT geomagnetic measurements. The measurement was done between 12 pm and 4 am in the same quiet location as in part C and the same methodology was used to verify that the geomagnetic measurement was comparable to LEMI-025.

Fig. 15 shows the geomagnetic field noise spectral density as measured by the magnetometer with an annealed sensor - we can see that in a low-noise location, it is actually possible to obtain 1 $pT_{rms}/\sqrt{Hz}$ at 1 Hz, which is an interesting result e.g. for magnetotelluric applications.

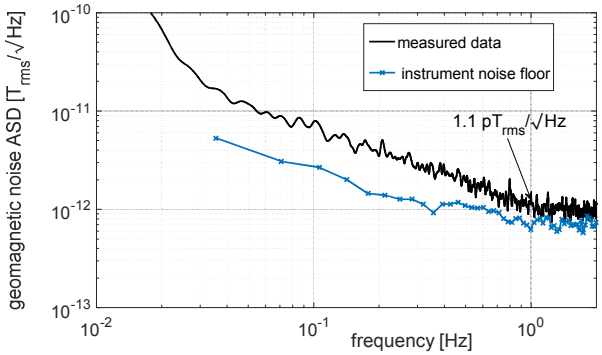

Fig. 15. Night-time (04/08/2019, 02-03 AM) geomagnetic measurement with the 1-pT magnetometer and an annealed sensor; instrument noise floor also shown, using the same data as of Fig. 10.

V. MAGNETOCARDIOGRAPHY EXPERIMENT

In order to perform measurements of the magnetic field of a human heart, we placed two magnetometer sensors on a marble plate located on top of a non-magnetic pillar. The measurements took place at the Budkov geomagnetic observatory of the Academy of Sciences of the Czech Republic, in South Bohemia. The two sensors were arranged as a transverse, dB_x/d_y gradiometer (with *x* denoting the sensor axis), the *y*-distance - or gradiometric base - was 12 cm (Fig. 16). The first sensor was located at the chest level and approximate heart position of the subject freely standing in front of it, whereas the second sensor was located towards the left side. Chest to sensor tip distance was about 4 to 5 cm.

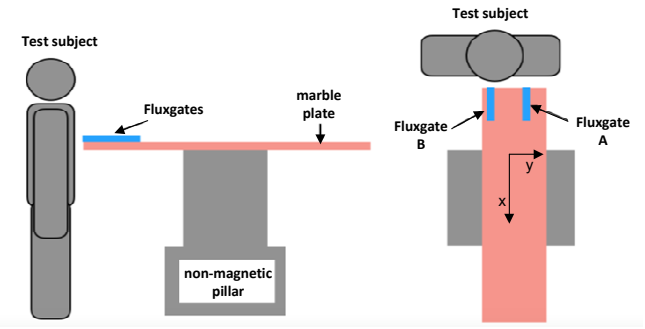

Fig. 16. Arrangement of the two fluxgate sensors for gradiometric MCG measurement. Gradiometric base was 12 cm.

The magnetometer was located at 1.5 m distance and powered by batteries. The magnetometer outputs were connected to the NI PXIe-4303 data acquisition module by 2-m long coaxial cables. In order to minimize the noise due to the digitizer range and noise, we selected the ± 0.1 V input range which corresponds to ± 450 nT. For this reason, the sensors were placed in E-W direction in front of the subject. Following the digitization of the magnetometer output at 1 kHz sampling rate, we applied a 30 Hz digital low pass filter, which is enough for the signal of a human heartbeat and removes 50 Hz effectively. The signals of both magnetometer channels (sensors) are shown in Fig. 17: the top trace corresponds to the sensor A (i.e. the sensor in front of the heart), whereas the bottom trace corresponds to the reference sensor B.

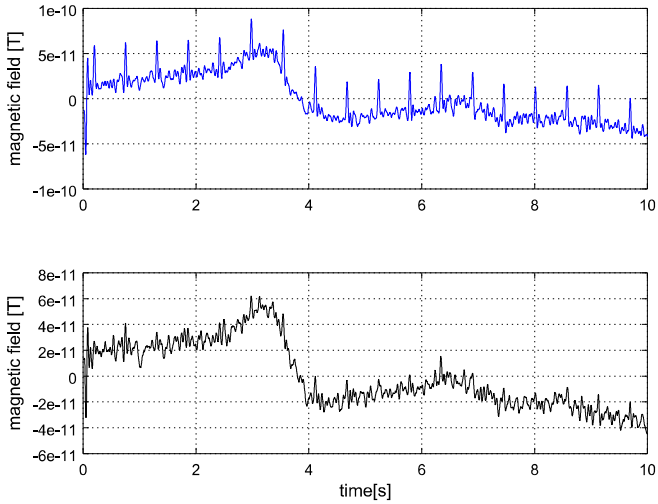

Fig. 17. Top: signal recorded by channel A (in front of the heart). Bottom: signal recorded by channel B.

As we can see, both signals share a common variation of magnetic field corresponding to the noise in the environment where the measurements took place. In addition to that, the first sensor shows also the peaks corresponding to the heart's magnetic field, which are missing in the signal measured by the second sensor.

When the signals from the two sensors are subtracted, the common variation of the magnetic field due to environmental noise is suppressed and the MCG signal is eventually revealed. In order to be sure that the peaks of magnetic field corresponded to the heartbeat, we simultaneously acquired ECG on the third channel of the data acquisition module, just by connecting two copper plates to the test subject hands. As

we can see in Fig. 18, the MCG signal obtained as difference of the two channels A and B corresponds to the ECG signal.

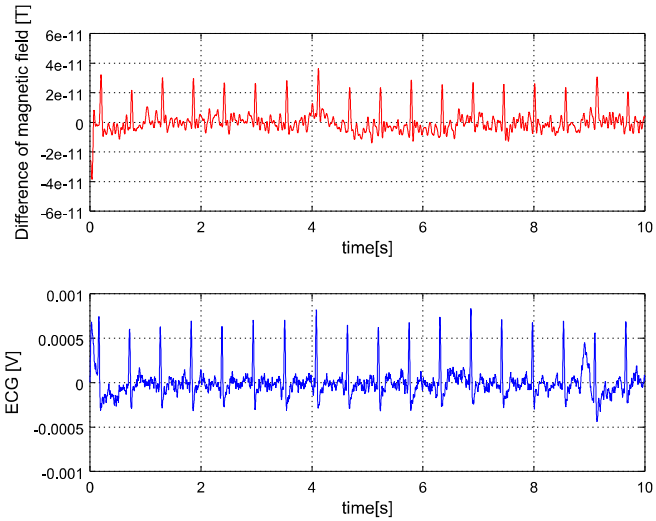

Fig. 18. Top: MCG signal obtained subtracting the recorded signals shown in Fig. 17. Bottom: ECG used a validation reference to confirm the heart origin of the MCG signal.

It must be noted that the MCG signal shown in Fig. 18 has been obtained without applying averaging, as opposed to other systems which rely on it in order to reduce the noise. We should also note that the subject was not secured to any support, and therefore was free to move. Despite the best effort to be stable, his position oscillated about 3 cm. In order to avoid the chest to touch the sensor we had therefore to keep the sensors about 4 to 5 cm from the chest of the test subject. This made the signal from the heart just about 20 - 25 pT peak, when typically it can reach even 100 pT. Therefore, with a better arrangement, we expect the signal-to-noise ratio to increase by a factor of four to five.

The signal-to-noise ratio is commonly improved by averaging at the cost of losing the dynamic information in a single-beat cycle. For instance, Fig. 19 shows a peak of MCG signal obtained by averaging 30 peaks recorded by our fluxgate gradiometer, without use of any synchronization by ECG (the peaks are large enough to allow easy detection and selection for averaging). We can identify not only the main peak but also the negative peak, which reaches -7 pT.

The efficiency of the gradiometer arrangement to suppress the environmental noise is illustrated in Fig. 20. The graph shows the spectral density of the fluxgate outputs without the MCG signal (the test subject was not present while the sensors were kept in the same arrangement). Both sensors show noise components, which are removed in their difference. Notably the spikes above 10 Hz are very efficiently suppressed. Unfortunately, however, the spike at 7.1 Hz is almost not affected by gradiometric arrangement. We believe it originated from magnetic field gradient signature of the electronic circuits (for instance the fan of the PXI frame) or from local EMI which coupled in a different way to both sensors.

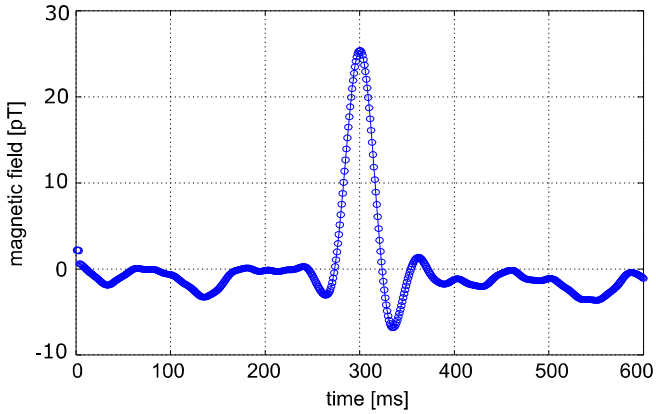

Fig. 19. MCG signal obtained when avearaging 30 peaks.

This was confirmed by the cross-spectral analysis (green trace in Fig. 20) which suppresses the signal at this particular frequency. Better arrangement of the instrument is expected to improve the rejection of this signal.

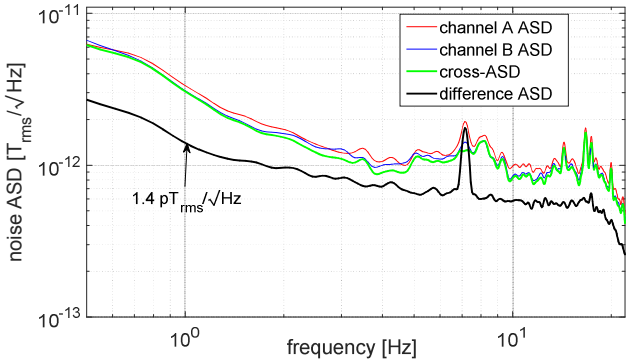

Fig. 20. – Noise ASD spectra of both individual channels and their difference (sensor arrangement as of Fig. 16). Also, the cross-power spectrum is shown (in amplitude units) indicating that most the observed noise is correlated, i.e. homogenous.

The noise density of the difference of the two channels is about 1.4 $pT_{rms}/\sqrt{Hz}$ at 1 Hz, which is slightly higher than the noise of the individual channels multiplied by $\sqrt{2}$ (1.41×0.75 $pT_{rms}/\sqrt{Hz}$, see Fig. 10) - we assume uncorrelated noise in both channels. This indicates that the suppression of the noise obtained by gradiometric configuration and numerical subtraction is not yet perfect, probably because of non-perfect alignment and calibration of the two probes. This might pose a problem in environments where the sources of local noise are larger and exhibit larger gradient.

VI. Conclusions

We have described the design of a portable magnetometer, based on a fundamental-mode, orthogonal fluxgate sensor, where 0.6 pT_{rms} white noise and 0.75 pT_{rms} noise density at 1 Hz can be achieved with an annealed sensor. This is to our knowledge so far the lowest published noise of a room-temperature vector magnetometer.

Even when considering the inherent sensor offset drift of −2.5 nT/K for the annealed sensor, the magnetometer can be utilized in a range of applications including biomedical measurements, where the frequency range of 10 mHz to 25 Hz is sufficient. We have also shown later that the offset drift can be successfully numerically compensated with a help of

an additional stable magnetometer, allowing even for geomagnetic measurements at much lower frequencies.

We have tested the instrument side-by-side to a state-of-the-art observatory magnetometer LEMI-025 and verified its low-noise performance during geomagnetic measurements. A comparison to HTS SQUID was also done, however in this case the SQUID exhibited high noise in the X-axis.

We have successfully demonstrated applicability of the instrument in a room-temperature, unshielded magnetocardiography, where even without averaging the MCG signal is clearly discernible. After the initial MCG experiment with search-coils [29] 56-years ago, magnetocardiography measurements were mostly limited to shielded rooms with SQUID magnetometers [30], because until now, the fluxgate magnetometers did not achieve noise figures better than few $pT_{rms}/\sqrt{Hz}$ at 1 Hz. Recently, optically-pumped magnetometers (OPM) have been used for MCG with noise figures about 50-300 $fT_{rms}/\sqrt{Hz}$ at 1 Hz [31]. Despite the noise of our fluxgate magnetometer still being higher than that of OPM devices, we believe in broadening the MCG usability not only by avoiding the necessity for cryogenic operation and expensive magnetic shields, but also by providing a simple and affordable sensor and electronics. However, when judging our MCG results, noisier environment than of the magnetic observatory has to be expected in reality and the common-mode rejection should be further improved. One possibility would be adding a (noisy, cheap) triaxial magnetometer close-by.

As the HTS SQUID sensors currently available state 0.2–0.6 $pT_{rms}/\sqrt{Hz}$ at 1 Hz [32], it is evident that the presented instrument meets HTS SQUID performance at least in terms of low-frequency noise. The future improvement of the 1-pT fluxgate magnetometer lies in its electronics where the closed-loop performance should be improved. Also, as we have shown, by further improving input stage common-mode rejection, with better shielding and differential amplification, we should be able to further decrease at least the noise of the electronics, if not of the complete magnetometer.

ACKNOWLEDGMENTS

This research was supported in part by the Czech Science Foundation (GA ČR) under Grant No. 16-10591Y "Magnetic gradiometer based on fundamental mode orthogonal fluxgate".

During his research fellowship at the Stellenbosch University, M.J. was supported by the mobility grant "International Mobility of Researchers in CTU", No CZ.02.2.69/0.0/0.0/16_027/0008465.

M.J. also thanks Danie Gouws for the support at SANSA and Emmanuel Nahayo for the observatory data. The authors acknowledge that a part of the electronic design was carried out by Vojtech Petrucha.

The results of the magnetocardiography experiments were presented at the Frontiers 2019 conference.

REFERENCES

[1] L. W. Pedersen, and L. Merenyi, "The FGE Magnetometer and the INTERMAGNET 1 Second Standard," J. Ind. Geophys. Union, vol 2, pp. 30-36, January 2016.

[2] J. Včelák, P. Ripka, and A. Zikmund, "Precise magnetic sensors for navigation and prospection," Journal of Superconductivity and Novel Magnetism, vol 28.3, pp. 1077-1080, 2015.

[3] Å. Forslund, S. Belyayev, N. Ivchenko, G. Olsson, T. Edberg, and A. Marusenkov, "Miniaturized digital fluxgate magnetometer for small spacecraft applications", Measurement Science and Technology, 19(1), 015202, 2007.

[4] A. D. Chave, and A. G. Jones, The magnetotelluric method: Theory and practice. New York: Cambridge University Press, pp. 445, 2012.

[5] R. Bazinet, A. Jacas, G. A. B. Confalonieri, and M. Vazquez, "A low-noise fundamental-mode orthogonal fluxgate magnetometer," IEEE Transactions on Magnetics, vol. 50, no. 5, pp. 1-3, May 2014.

[6] I. Mohanty, R. Nagendran, A. T. Arasu, R. Baskaran, and A. Mani, "Correlation of defect depth with diffusion time of eddy currents for the defects in conducting materials using transient eddy current NDE", Measurement Science and Technology, 29(10), 105601, 2018.

[7] B. W. Ficko, P. M. Nadar, P. J. Hoopes, S. G. Diamond, "Development of a magnetic nanoparticle susceptibility magnitude imaging array", Physics in Medicine & Biology, 59(4), 1047, 2014 .

[8] S Harada, I. Sasada, and F. Hang, "Development of a One‐Dimensional Fluxgate Array and Its Application to Magnetocardiogram Measurements," Electronics and Communications in Japan, vol. 98, no, 4, 2015, pp. 20-26, March 2015.

[9] C. Dolabdjian, S. Saez, A. Reyes Toledo and D. Robbes, "Signal-to-noise improvement of bio-magnetic signals using a flux-gate probe and real time signal processing,. Review of Scientific Instruments, vol. 69, no 10, pp.3678-3680, 1998.

[10] C. Hinnrichs, J. Stahl, K. Kuchenbrandt, and M. Schilling, "Dependence of sensitivity and noise of fluxgate sensors on racetrack geometry," IEEE Transactions on Magnetics, vol. 37, no. 4, pp. 1983-1985, 2001.

[11] M. Janosek , J. Vyhnánek, A. Zikmund, P. Butvin, and B. Butvinová, "Effects of core dimensions and manufacturing procedure on fluxgate noise," Acta Physica Polonica A, vol. 126, no. 1, pp. 104-105, 2014.

[12] Korepanov, V., & Marusenkov, A. (2012). Flux-gate magnetometers design peculiarities. Surveys in geophysics, 33(5), 1059-1079.

[13] R. H. Koch and J. R. Rozen, "Low-noise flux-gate magnetic-field sensors using ring-and rod-core geometries," Applied Physics Letters, vol. 78, no. 13, pp. 1897-1899, 2001.

[14] A. Marusenkov, "Possibilities of further improvement of 1 s fluxgate variometers," Geoscientific Instrumentation, Methods and Data Systems, vol. 6, no. 2, pp. 301-309, 2017.

[15] I. Sasada, "Orthogonal fluxgate mechanism operated with dc biased excitation," J . Appl. Phys., vol. 91, no. 10, pp. 7789, May 2002.

[16] D. P. Pappas, "High Sensitivity Magnetic Field Sensor Technology overview," unpublished lecture, NIST Boulder (2008), online: ftp://ftp.boulder.nist.gov/pub/pappas/MagneticSensors/Sensors.ppt, 2008.

[17] M. Butta, S. Yamashita, and I. Sasada, "Reduction of noise in fundamental mode orthogonal fluxgates by optimization of excitation current," IEEE Transactions on Magnetics, vol. 47, no. 10, pp. 3748-3751, 2011.

[18] M. Butta, and B.P. Schutte, "Low-noise Orthogonal Fluxgate using Flipped-Current Joule Annealing," IEEE Transactions on Magnetics, Vol. 55, Iss. 7, 2019.

[19] E. Weiss, and E. Paperno, "Noise investigation of the orthogonal fluxgate employing alternating direct current bias," J. Appl. Phys., vol. 109, no. 7, pp. 07E529, 2011.

[20] M. Butta, and I. Coroli, "Low offset drift–low-noise orthogonal fluxgate with synchronized polarity flipping," IEEE Trans. Magn., vol. 53, no. 4, April 2017

[21] N. Murata, H. Karo, I. Sasada, and T. Shimizu, "Fundamental Mode Orthogonal Fluxgate Magnetometer Applicable for Measurements of DC and Low-Frequency Magnetic Fields," IEEE Sensors Journal, vol. 18, no. 7, pp. 2705-2712, 2018.

[22] M. Janosek, M. Butta, E. Saunderson, D. Novotny, and C. Fourie, "1 pT-noise fluxgate magnetometer design and its performance in geomagnetic measurements," I2MTC 2019 Proceedings, 2019, accepted for publication

[23] M. Butta, and M. Janosek, "Very low frequency noise reduction in orthogonal fluxgate," AIP Advances, vol. 8, no. 4, pp. 047203, 2018.

[24] Janascard, “AD24USB / AD24ETH - Data acquisition modules”, online: http://www.janascard.cz/aj_Vyrobky.html (Accessed 20.11.2018)

[25] Janascard, “Noise reduction in AD24USB”, online: http://www.janascard.cz/PDF/AD24USBNoise.pdf (Accessed 01.08.2019)

[26] G. Waysand et al., “Seismo-ionosphere detection by underground SQUID in low-noise environment in LSBB – Rustrel, France,” European Physics Journal of Applied Physics, vol. 47, no. 1, pp.12705, 2009.

[27] L. J. Janse van Vuuren et al., “Implementation of an unshielded SQUID as a geomagnetic sensor,” in Proc. IEEE AFRICON 2013, Mauritius, pp. 908-912, 2013.

[28] S. Hong, J. H. Kim, A. Marusenkov, L. Hegymegi, and A. Csontos, “The Temperature Stability of LeMI-025 1-Second Variometer: Case Study in the Icheon Observatory”, Journal of Indian Geophysical Union, vol. 2, pp. 42-46, 2016.

[29] G. Baule et.al., "Detection of the magnetic field of the heart", American Heart Journal, Volume 66, Issue 1, 1963 (https://doi.org/10.1016/0002-8703(63)90075-9)

[30] D. Cohen et al., “Magnetocardiograms taken inside a shielded room with a superconducting point-contact magnetometer,” Appl. Phys. Lett. 16, pp. 278, 1970.

[31] O. Alem et al. “Fetal magnetocardiography measurements with an array of microfabricated optically pumped magnetometers," Physics in Medicine & Biology, Volume 60, Issue 12, p. 4797, 2015.

[32] Tristan Technlogies, “General Geophysical Devices”, online: http://tristantech.com/general (Accessed 26.11.2018)